Range Estimation and Performance Limits for UHF-RFID Backscatter Channels

Stefan Grebien, *Student Member, IEEE,* Josef Kulmer, *Student Member, IEEE,*
Florian Galler, *Student Member, IEEE,* Michael Goller, Erik Leitinger, *Member, IEEE,*
Holger Arthaber, *Member, IEEE,* and Klaus Witrisal, *Member, IEEE*

***Abstract*—The accuracy of time-of-flight based ranging over UHF RFID backscatter channels is fundamentally limited by the available bandwidth and highly dependent on the channel characteristics. Comprehensive wideband channel measurements are presented and analyzed with respect to parameters which influence the potential ranging performance. The Cramér Rao lower bound on time-of-flight based ranging is evaluated and we study the influence of dense multipath on the bound. Based on a line-of-sight (LOS) plus dense multipath (DM) radio channel model, a multiple-input multiple-output (MIMO) ranging algorithm is developed, capable of iteratively estimating the LOS parameters and the statistics of the DM. The accuracy of the developed algorithm is compared to the performance bound. The results highlight the tradeoff between a higher bandwidth and spatial diversity for UHF RFID systems with respect to time-of-flight based ranging. In a 2×2 MIMO setup, an accuracy of about $0.5\,\mathrm{m}$ is achieved at a bandwidth of $50\,\mathrm{MHz}$.**

***Index Terms*—UHF-RFID, backscatter channel, Cramér-Rao bound, dense multipath channels, ranging, MIMO.**

I. Introduction

ACCURATE and robust ranging with ultra-high frequency (UHF) radio frequency identification (RFID) tags is a key-enabler for a variety of applications in production, supply chain management, and retail. Many of these require a sub-meter accuracy which is still an unsolved challenge. For time-of-flight (ToF) based ranging systems, the available bandwidth imposes a fundamental limit on the achievable accuracy.

A thorough characterization of the UHF-RFID channel is needed for developing robust ranging algorithms. For narrowband signals, the backscatter channel has been well analyzed with respect to fading statistics [1]. Several measurement campaigns [1]–[5] have studied the individual (*i.e.* up- and downlink) channels in both the narrowband and wideband regimes, but only some analyses have been performed of wideband parameters like the Rician K-factor for the line-of-sight (LOS) component or the root-mean-square (RMS) delay spread for the backscatter channel [2].

The application driven requirement of sub-meter ranging leads to a clear trend towards larger bandwidth systems in the UHF-RFID technology [6]–[8]. Ranging methods are heavily influenced by the wideband statistics of the backscatter channel. The achievable ranging performance has been analyzed for different scenarios. E.g., in ultra-wideband settings the Cramér Rao lower bound and the Ziv-Zakai bound have been derived [9], [10]. The Cramér Rao lower bound in dense multipath (DM) channels has been studied in [11] for ToF-based ranging, and in [8] for a wideband UHF-RFID scenario.

To exploit the utmost ranging information from channel measurements, high accuracy channel estimators are necessary. Maximum likelihood estimators for superimposed signals are typically iterative algorithms, e.g., the expectation maximization (EM) algorithm [12] which evolved into space alternating EM schemes [13]. These algorithms assume separable superimposed signals in additive white Gaussian noise (AWGN). Measurements showed [4], [14], [15] that due to overlapping of the signals and a restricted measurement aperture an additional interference term, so-called DM, needs to be introduced in the channel model. This means that a high-performance channel estimator should consider this impairment [14].

Taking into account the requirements and the current state of the research, the main contributions of this paper are:[1]

- we develop a multiple-input multiple-output (MIMO) channel estimator capable of estimating the LOS parameters (delay, angle-of-departure, angle-of-arrival) and the statistics of the DM by utilizing a delay-sum beamformer, and
- we analyze measurements from two scenarios, apply the developed algorithm and analyze the ranging error bound for backscatter channels under DM, in single-input single-output (SISO) and MIMO setups.

The paper is organized as follows: Section II defines the problem and introduces the channel model. Section III develops range estimators for the SISO and MIMO setup and presents their Cramér Rao lower bounds. Section IV describes the measurement setup and Section V analyzes the measured data. In Section VI the algorithms are validated with simulated and measured data and Section VII concludes the paper.

II. Problem Formulation

We investigate the backscatter channel consisting of a downlink channel from RFID reader ℓ to an RFID tag and

This work was performed within the project REFlex, funded by the Austrian Research Promotion Agency (FFG; project number: 845630).

S. Grebien, J. Kulmer, E. Leitinger, and K. Witrisal are with the Signal Processing and Speech Communication Laboratory, Graz University of Technology, A-8010 Graz, Austria (e-mail: stefan.grebien@tugraz.at).

F. Galler, and H. Arthaber are with the Institute of Electrodynamics, Microwave and Circuit Engineering, TU Wien, A-1040 Vienna, Austria.

M. Goller is with Detego GmbH, A-8020 Graz, Austria.

[1]Parts of this journal paper have been presented at the IEEE RFID conference 2017 [16]. In Section II we adapted the channel model to be able to cope with the development of the MIMO range estimator, which is found in Section III-B, and the ranging error bound for the MIMO setup in Section III-C2. Finally, we added simulation results in Section VI-A and applied the developed algorithm to the measured data in Section VI-B2.

an uplink from the tag to the RFID reader ℓ'.[2] Both RFID readers ℓ and ℓ' are equipped with K and K' closely spaced antennas respectively. Antennas with index k are assigned to reader ℓ located at $\mathbf{p}_{\ell k}$ and antennas with index k' belong to ℓ' at $\mathbf{p}_{\ell' k'}$. The tag is located at unknown position $\mathbf{p}$.

Each of the RFID reader antennas can be used to transmit and/or receive a wideband signal [6], [8]. The aim is to find the overall propagation delay of the backscatter channel between the transmitting RFID reader via the tag to the receiving RFID reader. Depending on the number of antennas used at the transmitting and receiving RFID reader, a SISO, a SIMO or a MIMO system can be analyzed.

A. Channel Model

The backscatter channel model between downlink antenna k and uplink antenna k' is modeled by a LOS plus DM model [2], [11]

$$h_{kk'}(\tau) = \alpha_{kk'}\delta(\tau - \tau_{kk'}) + \nu_{kk'}(\tau), \tag{1}$$

where $\delta(\tau)$ is the Dirac pulse, and the LOS is characterized by its complex-valued amplitude $\alpha_{kk'}$ and delay $\tau_{kk'}$. The LOS delay of the backscatter channel is equivalent to the Euclidean distance between the positions of the downlink antenna, the tag and the uplink antenna scaled by the speed of light c, such that $\tau_{kk'} = (\|\mathbf{p}_{\ell k} - \mathbf{p}\| + \|\mathbf{p} - \mathbf{p}_{\ell' k'}\|)/c$.

The term $\nu_{kk'}(\tau)$ in (1) models the DM consisting of all occurring multipath components (MPC), including reflections at flat surfaces and scattering at small objects. This DM is modeled as a zero-mean complex Gaussian random process, assuming uncorrelated scattering (US) along the delay axis τ [17]. Thus, the auto-correlation function of the DM is $\mathbb{E}\{\nu_{kk'}(\tau)[\nu_{kk'}(u)]^*\} = S_{\nu,kk'}(\tau - \tau_{kk'})\delta(\tau - u)$ with $S_{\nu,kk'}(\tau)$ as the power-delay-profile (PDP) of the DM which is zero for $\tau < 0$. This means, that some information about the LOS delay is encoded in the PDP of the DM. In this work we use a double exponential PDP [4] which includes five parameters $\mathbf{\Gamma} = [\tau_{\text{DM}}, P_{\text{DM}}, \gamma_{\text{fall}}, \gamma_{\text{rise}}, \chi]^T$, where τ_{DM} is the onset of the DM, P_{DM} describes the overall power of the DM, γ_{rise}, γ_{fall}, and χ are shape parameters of the DM.[3] We also assume quasi-stationarity in the spatial domain, meaning that for one reader / tag configuration, the PDP does not change noticeably in the vicinity of the tag [17]. The signal model does not include more than one tag. This does not limit the system operation to one tag, but rather implies the usage of multiple access schemes [6], [7] to separate multiple tags.

B. Received Signal

The received signal $r_{kk'}(t)$[4] at any antenna k' stemming from antenna k results as convolution of the transmitted baseband signal $s(t)$ and the overall backscatter channel described in (1) as

$$\begin{aligned} r_{kk'}(t) =& \alpha_{kk'} s(t - \tau_{kk'}) \exp\{-j\,(2\pi f_c \tau_{kk'} + \varphi_0)\} \\ &+ (s * \nu_{kk'})(t) + \omega(t), \end{aligned} \tag{2}$$

where φ_0 is an unknown initial phase and $\omega(t)$ is AWGN with a two-sided power spectral density of $N_0/2$.

III. Range Estimation

Depending on the number of used antennas at the transmitting and receiving reader, different estimators are developed in the following section.

A. Single-Input Single-Output

The range measurement obtained between a transmit reader antenna, the tag, and a receive reader antenna is given by $d_{\text{SISO}} = c\tau_{kk'}$, determining the unknown tag position $\mathbf{p}$ as a point on an ellipse. By sampling the received signal with $f_{\text{s}} = 1/T_{\text{s}}$, with T_{s} as sampling period, (2) can be written for the SISO model in vector notation as

$$\mathbf{r}_{kk'} = \alpha_{kk'}\mathbf{s}_{\tau_{kk'}} + \mathbf{n}_{\text{c},kk'} + \boldsymbol{\omega}_{kk'} \tag{3}$$

where $\mathbf{s}_{\tau_{kk'}} = [s(-\tau_{kk'}), s(T_{\text{s}} - \tau_{kk'}),\ \dots\ , s((N-1)T_{\text{s}} - \tau_{kk'})]^T \exp\{-j\,(2\pi f_c \tau_{kk'} + \varphi_0)\}$, $\mathbf{n}_{\text{c},kk'} = [(s*\nu_{kk'})(0), (s*\nu_{kk'})(T_{\text{s}}),\ \dots\ , (s*\nu_{kk'})((N-1)T_{\text{s}})]^T$, and $\mathbf{r}_{kk'}$ and $\boldsymbol{\omega}_{kk'}$ are sampled versions of the received signal and the AWGN as vectors $\in \mathbb{C}^{N\times 1}$.

Given the deterministic unknown parameter vector $\boldsymbol{\theta}_{\text{SISO}} = [\tau_{kk'}, \alpha_{kk'}]^T$, the likelihood function is given as

$$\begin{aligned} f(\mathbf{r}_{kk'}|\boldsymbol{\theta}_{\text{SISO}}) \propto \exp\big\{&(\mathbf{r}_{kk'} - \alpha_{kk'}\mathbf{s}_{\tau_{kk'}})^H \\ &\times \mathbf{C}_{kk'}^{-1}(\mathbf{r}_{kk'} - \alpha_{kk'}\mathbf{s}_{\tau_{kk'}})\big\}, \end{aligned} \tag{4}$$

where $\mathbf{C}_{kk'} = \mathbf{S}^H\mathbf{S}_{\boldsymbol{\nu},kk'}\mathbf{S} + \frac{N_0}{T_{\text{s}}}\mathbf{I} \in \mathbb{R}^{N\times N}$ is the covariance matrix with $\mathbf{S} = [\mathbf{s}_0,\ \dots\ , \mathbf{s}_{(N-1)T_{\text{s}}}]^T$ and $\mathbf{S}_{\boldsymbol{\nu},kk'} = \text{diag}\{S_{\nu,kk'}(iT_{\text{s}})\cdot T_{\text{s}}\}$ is a diagonal matrix containing the PDP.

To estimate the distance d_{SISO}, we apply: (i) a maximum likelihood (ML) estimator, and (ii) a naïve matched filter (MF) estimator. The ML estimator accounts for the influence of the DM expressed by the covariance matrix and thus requires the PDP of the DM and N_0 to be known.

1) ML estimator: The ML estimator for the delay estimation problem is found by maximizing the likelihood function (4) with respect to the parameter $\tau_{kk'}$.

$$\hat{d}_{\text{SISO,ML}} = c \cdot \underset{\tau_{kk'}}{\text{argmax}}\{f(\mathbf{r}_{kk'}|\boldsymbol{\theta}_{\text{SISO}})\}. \tag{5}$$

The nuisance parameter $\alpha_{kk'}$ has to be estimated jointly with $\tau_{kk'}$ [20], which can be written as

$$\hat{\alpha}_{kk'}(\tau_{kk'}) = \frac{\mathbf{r}_{kk'}^H\mathbf{C}_{kk'}^{-1}\mathbf{s}_{\tau_{kk'}}}{\mathbf{s}_{\tau_{kk'}}^H\mathbf{C}_{kk'}^{-1}\mathbf{s}_{\tau_{kk'}}}. \tag{6}$$

2) MF estimator: The MF estimator simply correlates the received signal with the transmit pulse and searches for the maximum, i.e.

$$\hat{d}_{\text{SISO,MF}} = c \cdot \underset{\tau_{kk'}}{\text{argmax}}\{\mathbf{r}_{kk'}^H\mathbf{s}_{\tau_{kk'}}\}. \tag{7}$$

This estimator ($\hat{d}_{\text{SISO,MF}}$) would be optimal for a signal model without the DM [20, p. 192].

[2]This can describe either a monostatic setup ($\ell = \ell'$) or a bistatic setup ($\ell \neq \ell'$).

[3]It is straightforward to use different PDPs, e.g. an exponential PDP, since only the parameter vector $\mathbf{\Gamma}$ has to be adjusted.

[4]This model assumes perfect (frequency independent) backscattering of the tag over the whole bandwidth. This certainly does not hold when considering 'wideband' signals, but the smaller the bandwidth gets, the less frequency dependent the radar cross section of a tag gets [18]. It would be possible to include the frequency dependent behavior in the baseband pulse $s(t)$ [19], but in this work we want to focus on the influence of the channels, and thus neglect this effect.

B. Multiple-Input Multiple-Output

To overcome the shortcoming of the SISO range estimation, namely the *need to know* the statistics of the DM plus AWGN, a SIMO or MIMO setup is necessary which enables the joint estimation of the LOS parameters and the parameters of the DM.[5]

The received signal in a MIMO setup is found by stacking the individual received signals between an RFID reader via the tag to an RFID reader. The received signal $\mathbf{r}$ reads

$$\mathbf{r} = \alpha\mathbf{s} + \mathbf{n}_{\mathrm{c}} + \boldsymbol{\omega} \quad \in \mathbb{C}^{NKK'\times 1}, \tag{8}$$

where $\mathbf{r} = [\mathbf{r}_{11}^T, ..., \mathbf{r}_{KK'}^T]^T$, $\mathbf{s} = [\mathbf{s}_{11}^T, ..., \mathbf{s}_{KK'}^T]^T$, $\mathbf{n}_{\mathrm{c}} = [\mathbf{n}_{\mathrm{c},11}^T, ..., \mathbf{n}_{\mathrm{c},KK'}^T]^T$, and $\boldsymbol{\omega} = [\boldsymbol{\omega}_{11}^T, ..., \boldsymbol{\omega}_{KK'}^T]^T$. We assume that the transmitting and receiving antennas are spaced closely enough such that the amplitude $\alpha = \alpha_{kk'} \forall k, k'$ is the same over all individual backscatter channels.

To reduce the $K \times K'$ large search space for the individual delays $\tau_{kk'}$, they are re-written as a sum of three terms: (i) a delay from the center of the transmitting array $\mathbf{p}_\ell$ via the tag to the center of the receiving array $\mathbf{p}_{\ell'}$, $\tau_{\ell\ell'} = \frac{1}{c}(||\mathbf{p} - \mathbf{p}_\ell||^2 + ||\mathbf{p} - \mathbf{p}_{\ell'}||^2) = \frac{1}{c} d_{\mathrm{MIMO}}$, (ii) an additional delay $\Delta\tau_{\ell k} = -\frac{1}{c}(\Delta p_{x_{\ell k}} \cos(\varphi_{\mathrm{AoD}}) + \Delta p_{y_{\ell k}} \sin(\varphi_{\mathrm{AoD}}))$ as a function of the angle-of-departure φ_{AoD} and the known antenna position offsets $\Delta\mathbf{p}_{\ell k}$ given by the transmitter array geometry, and (iii) an additional delay $\Delta\tau_{\ell' k'} = -\frac{1}{c}(\Delta p_{x_{\ell' k'}} \cos(\varphi_{\mathrm{AoA}}) + \Delta p_{y_{\ell' k'}} \sin(\varphi_{\mathrm{AoA}}))$ as a function of the angle-of-arrival φ_{AoA} and the known antenna position offsets $\Delta\mathbf{p}_{\ell' k'}$ given by the receiver array geometry.[6] The parameters of the LOS are combined into the vector $\boldsymbol{\psi} = [\tau_{\ell\ell'}, \varphi_{\mathrm{AoD}}, \varphi_{\mathrm{AoA}}]^T$

The according likelihood function for the received signal, given the unknown deterministic parameter vector $\boldsymbol{\theta}_{\mathrm{MIMO}} = [\boldsymbol{\psi}, \alpha, \boldsymbol{\eta}]^T$, is

$$f(\mathbf{r}|\boldsymbol{\theta}_{\mathrm{MIMO}}) = \frac{1}{\pi^{NKK}|\mathbf{C}(\boldsymbol{\eta})|} \exp\Big\{(\mathbf{r} - \alpha\mathbf{s}(\boldsymbol{\psi}))^H \times \mathbf{C}(\boldsymbol{\eta})^{-1}(\mathbf{r} - \alpha\mathbf{s}(\boldsymbol{\psi}))\Big\}, \tag{9}$$

where we have introduced $\mathbf{s}(\boldsymbol{\psi})$ to show the dependence of the delay, and the two angles explicitly.[7] As for the amplitudes, we assume that the statistics of the DM process do not change for one reader / tag configuration, thus $\mathbf{C}_{kk'}(\boldsymbol{\eta}) \approx \tilde{\mathbf{C}}(\boldsymbol{\eta})$, with $\boldsymbol{\eta} = [N_0, \boldsymbol{\Gamma}]^T$ as the parameters describing the AWGN and the parameters of the DM process. The overall covariance matrix can now be written as a diagonal block matrix $\mathbf{C}(\boldsymbol{\eta}) = \mathrm{diag}(\tilde{\mathbf{C}}(\boldsymbol{\eta}), ..., \tilde{\mathbf{C}}(\boldsymbol{\eta}))$.[8]

The direct maximization of the likelihood function (9) to derive an ML estimator for $\boldsymbol{\theta}_{\mathrm{MIMO}}$ is difficult, since a maximization with respect to eleven parameters[9] would be necessary. To split the search space into smaller search spaces, a structured mean field variational approach is used which approximates the posterior of the parameters as

$$f(\boldsymbol{\theta}_{\mathrm{MIMO}}|\mathbf{r}) \approx q(\boldsymbol{\psi})q(\alpha)q(\boldsymbol{\eta}) = q(\boldsymbol{\theta}_{\mathrm{MIMO}}), \tag{10}$$

where we assumed that the DM process, the parameters of the LOS component, and the complex amplitudes are independent. As no prior information of the parameters is available, a uniform prior is used for the parameters, meaning that the parameter posterior is proportional to the likelihood. To find a close approximation for the parameter posterior we chose to minimize the Kullback-Leibler divergence from the parameter posterior $f(\boldsymbol{\theta}_{\mathrm{MIMO}}|\mathbf{r})$ towards $q(\boldsymbol{\theta}_{\mathrm{MIMO}})$. This can be accomplished [21] by maximizing the variational lower bound of q towards the joint probability density function $f(\boldsymbol{\theta}_{\mathrm{MIMO}}, \mathbf{r})$

$$\mathcal{L}(q) = \int q(\boldsymbol{\theta}_{\mathrm{MIMO}}) \log \frac{f(\boldsymbol{\theta}_{\mathrm{MIMO}}, \mathbf{r})}{q(\boldsymbol{\theta}_{\mathrm{MIMO}})} d\boldsymbol{\theta}_{\mathrm{MIMO}}. \tag{11}$$

By evaluating the variational lower bound for the individual subsets of parameters while keeping the other parameters fixed, using a point estimate for the parameters $q(\boldsymbol{\psi}) = \delta(\boldsymbol{\psi} - \hat{\boldsymbol{\psi}})$, an iterative local maximization of the variational lower bound can be found. In the appendix, the derivation of the maximization problems can be found for the different subsets. At each iteration step we update the LOS parameters delay, the angle-of-arrival (AoA), and the angle-of-departure (AoD) using the log likelihood in (9) conditioned on the LOS amplitude and covariance from the previous iteration

$$\hat{\boldsymbol{\psi}}^{\mathrm{new}} = \underset{\hat{\boldsymbol{\psi}}}{\mathrm{argmax}} \Big\{ -\Big(\mathbf{r} - \hat{\alpha}^{\mathrm{old}}\mathbf{s}(\hat{\boldsymbol{\psi}})\Big)^H \mathbf{C}(\hat{\boldsymbol{\eta}}^{\mathrm{old}})^{-1} \times \Big(\mathbf{r} - \hat{\alpha}^{\mathrm{old}}\mathbf{s}(\hat{\boldsymbol{\psi}})\Big)\Big\}, \tag{12}$$

followed by updating the LOS amplitude and the noise statistic parameters[10]

$$\hat{\alpha}^{\mathrm{new}} = \frac{\mathbf{r}^H \mathbf{C}(\hat{\boldsymbol{\eta}}^{\mathrm{old}})^{-1} \mathbf{s}(\hat{\boldsymbol{\psi}}^{\mathrm{new}})}{\mathbf{s}(\hat{\boldsymbol{\psi}}^{\mathrm{new}})^H \mathbf{C}(\hat{\boldsymbol{\eta}}^{\mathrm{old}})^{-1} \mathbf{s}(\hat{\boldsymbol{\psi}}^{\mathrm{new}})}, \tag{13}$$

$$\hat{\boldsymbol{\eta}}^{\mathrm{new}} = \underset{\hat{\boldsymbol{\eta}}}{\mathrm{argmax}} \Big\{ -\log\{|\mathbf{C}(\hat{\boldsymbol{\eta}})|\} - \Big(\mathbf{r} - \hat{\alpha}^{\mathrm{new}}\mathbf{s}(\hat{\boldsymbol{\psi}}^{\mathrm{new}})\Big)^H \mathbf{C}(\hat{\boldsymbol{\eta}})^{-1} \Big(\mathbf{r} - \hat{\alpha}^{\mathrm{new}}\mathbf{s}(\hat{\boldsymbol{\psi}}^{\mathrm{new}})\Big) \Big\}. \tag{14}$$

Due to the sequential nature of the algorithm it needs initial values for all parameters. These can be found for the LOS parameters by a grid search for the delay (spacing of T_s), the AoA and AoD (spaced by 5°) with a matched filter delay-sum beamformer, for the AWGN parameters by estimating $\hat{N}_0$ according to (28) and using standard values for the DM parameters.[11] A summary of the algorithm is presented in Algorithm 1.

[5] In the following the MIMO estimator is developed which can be applied straightforwardly to a SIMO setup by neglecting the angle-of-departure that cannot be estimated by an RFID SIMO setup.

[6] For (ii) and (iii) it is assumed that the distance between the tag and the transmitter/receiver array is large with respect to the array spacing.

[7] We could have modeled the parameter vector $\boldsymbol{\psi}$ also as a function of the unknown tag position $\mathbf{p}$, but as we are interested in ranging we estimate the delay $\tau_{\ell\ell'}$ directly.

[8] This diagonal block matrix assumes, that the DM at different antenna elements are uncorrelated. In Section V the spaced-distance-correlation-function for the DM is analyzed, which expresses these correlations.

[9] For the direct search, the real and imaginary part of the amplitude have to be searched for separately

[10] As we are interested most in the LOS parameters we update these parameters first. Depending on the order of the update, the algorithm will sometimes converge to a different local maxima [21].

[11] As the DM can only start after the LOS arrived at the receiver, we set $\tau_{\mathrm{DM,init}} = \hat{\tau}_{\ell,\ell'}$, we assume that the power in the DM is approximately half the overall noise power, use standard values [4] for $\gamma_{\mathrm{rise}} = 20$ ns and $\gamma_{\mathrm{fall}} = 8$ ns and initialize the shape parameter χ randomly in the interval $(0, 1)$.

Algorithm 1: Summary of the proposed algorithm.

Initialization:

- perform grid search for $\hat{\boldsymbol{\psi}} = \operatorname{argmax}_{\boldsymbol{\psi}} \left\{ \mathbf{r}^H \mathbf{s}(\boldsymbol{\psi}) \right\}$
- estimate $\hat{N}_0$ according to (28) and initialize $\hat{\boldsymbol{\eta}} = [\hat{N}_0/2, \hat{\boldsymbol{\Gamma}}]^T$ (cf. Footnote 11) and $\hat{\alpha}$ acc. to (13)

Iterations:

do

update $\hat{\boldsymbol{\psi}}$ according to (12)
update $\hat{\alpha}$ according to (13)
update $\hat{\boldsymbol{\eta}}$ according to (14)

while *not converged*;

C. Ranging Error Bound $\mathcal{R}(\tau)$

1) REB for SISO processing: The Cramér Rao lower bound for the delay estimation problem for DM channels [11], called ranging error bound (REB), is given by the inverse of the square root of the equivalent Fisher information (EFI),

$$\mathcal{R}(\tau_{kk'}) = \sqrt{\mathcal{I}_{\tau_{kk'}}^{-1}}. \tag{15}$$

For a backscatter channel the EFI is

$$\mathcal{I}_{\tau_{kk'}} = 8\pi^2 \beta^2 \widetilde{\mathrm{SINR}}_{kk'} + \mathrm{tr}\left\{ \mathbf{C}_{kk'}^{-1} \frac{\partial \mathbf{C}_{kk'}}{\partial \tau} \mathbf{C}_{kk'}^{-1} \frac{\partial \mathbf{C}_{kk'}}{\partial \tau} \right\}, \tag{16}$$

$$\approx 8\pi^2 \beta^2 \widetilde{\mathrm{SINR}}_{kk'} \tag{17}$$

where $\beta^2 = \|\dot{\mathbf{s}}_{\tau_{kk'}}\| / (4\pi^2 \|\mathbf{s}_{\tau_{kk'}}\|)$ is the effective (mean-square) bandwidth of the transmit pulse, $\dot{\mathbf{s}}_{\tau_{kk'}}$ is the derivative of $s(t - \tau_{kk'})$ with respect to t, and $\widetilde{\mathrm{SINR}}_{kk'}$ is the effective signal-to-interference-plus-noise-ratio (SINR) [8]. The second term in (16) describes the additional delay information in the DM, as the onset of the DM coincides with the LOS delay.[12]

In particular, the effective SINR describes the useful ranging information of the LOS component when influenced by DM and AWGN and can be factored into three parameters [11]:

(i) the signal-to-interference-plus-noise-ratio $\mathrm{SINR}_{kk'} = |\alpha_{kk'}|^2 \mathbf{s}_{\tau_{kk'}}^H \mathbf{C}_{kk'}^{-1} \mathbf{s}_{\tau_{kk'}}$ which quantifies the signal-to-noise-ratio (SNR) after the square root of the covariance matrix has been applied as whitening filter,

(ii) the whitening gain $\gamma_{kk'} = \frac{\dot{\mathbf{s}}_{\tau_{kk'}}^H \mathbf{C}_{kk'}^{-1} \dot{\mathbf{s}}_{\tau_{kk'}}}{\mathbf{s}_{\tau_{kk'}}^H \mathbf{C}_{kk'}^{-1} \mathbf{s}_{\tau_{kk'}}} \frac{1}{4\pi^2 \beta^2}$ which quantifies the bandwidth gain due to the knowledge of the PDP,

(iii) and $\sin^2(\varphi_{kk'})$ which is an information loss due to the estimation of the nuisance parameter $\alpha_{kk'}$.[13]

2) REB for MIMO processing: In [8] we have shown that the EFI is additive for individual measurements if the statistics of the DM are known and the antenna elements within one array are closely spaced, leading to

$$\mathcal{I}_{\tau_{\ell\ell'}} = \sum_{k=1}^{K} \sum_{k'=1}^{K'} \mathcal{I}_{\tau_{kk'}}, \text{ and} \tag{18}$$

$$\mathcal{I}_{\tau_{\ell\ell}} = \sum_{k=1}^{K} \sum_{k'=k}^{K} \mathcal{I}_{\tau_{kk'}} \tag{19}$$

for a bistatic (18) and a monostatic (19) setup respectively. For the algorithm developed in Section III-B this EFI is overrated, as the estimation process of the AoA, the AoD and the DM parameters are not accounted for in the derivation of (16) and (17). The estimation of additional parameters shows to be subtractive with respect to the EFI [20]. Thus, the REB computed from (18) or (19) is certainly a lower bound for Algorithm 1. While (19) and (18) are developed for non-coherent processing of the measurements, it is discussed in [11] that for the assumption of a uniformly distributed PDP in angular domain they also hold for coherent processing. Eq. (18) or (19) can be interpreted as the REB for a MIMO setup with knowledge of the PDP as well as the AoD and AoA.

In Section VI we compare the performance of the derived ranging algorithms with the theoretical lower bound, obtained from the signal model, for both SISO and MIMO processing. Furthermore, we evaluate the impact of the estimated PDP, AoD and AoA on the REB for MIMO processing. Next, the measurement scenarios are described and basic channel parameters are analyzed.

IV. Measurement Setup

The measurement data used in this work are obtained from a series of wideband measurements using an m-sequence channel sounder by Ilmsens [22], operating in the frequency range (-10 dB cut-off) from 0.1 to 3.2 GHz. It has one transmitting (TX) and two receiving channels (RX), a sampling frequency of 6.95 GHz, thus a resolution of 4.31 cm. It uses a sequence length of 4095 chips and thus a maximum delay of 589.2 ns or 176.6 m. To measure up to four antennas per RX channel we use two RF switching matrices [23]. The cross-talk and the system-response of the measurement equipment are removed up to the antenna ports by a match-through calibration. This setup provides the flexibility to study different configurations, including SISO as well as MIMO setups.

A tapered slot antenna (also called Vivaldi antenna) with a 3 dB mainlobe width of approximately $90\,^\circ$ is used as reader antenna. Its wideband gain pattern is not completely independent of frequency but shows good properties in the frequency range from 0.75 to 1.5 GHz. The tag antenna is an elliptic dipole-like structure with an omnidirectional gain pattern similar to RFID tags. Again, the wideband pattern shows good properties in the same frequency range as the reader antennas.

A positioning table is used to accurately position the RFID tag in an automated way to obtain a large number of measurements with different tag positions. The positioning table spans a 0.68×0.64 m grid with a spacing of 4 cm. For the

[12] In (10) we assumed independence among $\tau_{kk'}$ and τ_{DM} yielding the compact algorithm in (12) and (14). This assumptions affects the information contained in $\tau_{kk'}$ and subsequently the potential performance of the estimator.

[13] $\varphi_{kk'}$ describes the angle between the whitened pulse and the whitened pulse derivative in a vector space. For common pulses and an AWGN model, $\varphi_{kk'} = 90°$. Due to the whitening this angle gets smaller than $90°$.

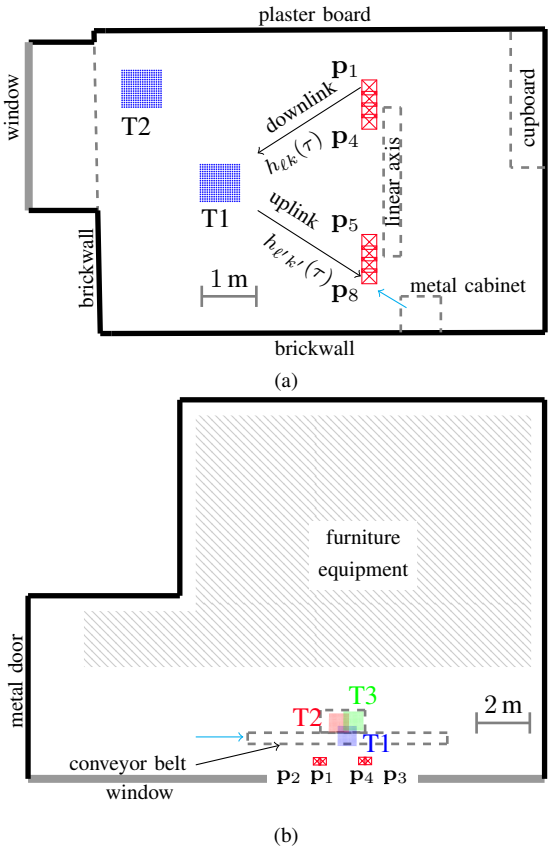

Fig. 1. Floorplans of the two measurement scenarios. At each table position, 306 measurements are obtained with a spacing of 4 cm on a 17×18 grid. The cyan arrows depict the point of view of the photographs in Fig. 2.
(a) Scenario A: Laboratory at TU Wien with some furniture and a linear axis. Eight closely-spaced Vivaldi antennas arranged as two arrays ($\mathbf{p}_1$ to $\mathbf{p}_4$ & $\mathbf{p}_5$ to $\mathbf{p}_8$) and two different table positions (T1 & T2).
(b) Scenario B: Industrial setup with a conveyor belt, aluminum profiles, and many scatterers. Four closely-spaced Vivaldi antennas arranged as two arrays ($\mathbf{p}_1$ and $\mathbf{p}_2$ & $\mathbf{p}_3$ and $\mathbf{p}_4$) and three different table positions (T1, T2 & T3).

individual measurement runs, the positioning table can be placed at different locations in the room in order to evaluate the desired coverage.

Measurement data have been acquired in two different scenarios: Scenario A is a standard laboratory hall at TU Wien that was chosen in order to evaluate a typical indoor lab / office environment. Scenario B is an industrial hall with a significant amount of metal fixtures. Both scenarios are described in more detail in the following sections.

A. Scenario A

In Fig. 1a and Fig. 2a the floorplan and a picture of the measurement scenario in the laboratory are depicted, respectively. The positioning table with the tag antenna is placed at two positions in the room (T1 & T2), while the reader antennas are set up as two linear arrays with antenna positions at $\mathbf{p}_1$ to $\mathbf{p}_4$ & $\mathbf{p}_5$ to $\mathbf{p}_8$. The back of the room holds a cabinet with laboratory equipment, while the other side of the room is occupied by a metal cabinet. Furthermore, the lab holds a set of aluminum profiles for linear axis movements that is placed directly behind the antennas. All antennas are set up at a constant height of 1.3 m.

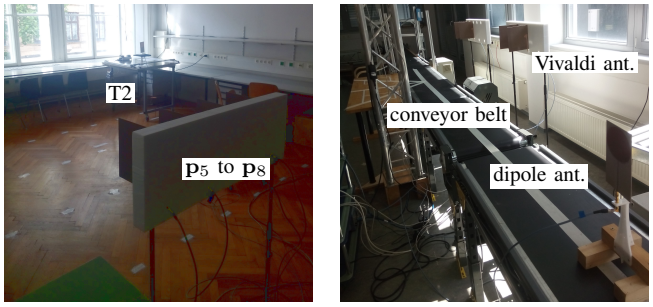

(a) (b)

Fig. 2. Pictures of the two measurement scenarios: (a) Scenario A, (b) Scenario B. The point of view with respect to the floorplan is shown with a cyan arrow in Fig. 1.

B. Scenario B

The second measurement campaign (see floorplan in Fig. 1b and picture in Fig. 2b) has been performed in an industrial hall with metal fixtures and a conveyor belt setup as typically found in manufacturing and logistics. The hall is approximately 18 by 12 m large and the facilities are used to analyze and study logistic processes and systems, e.g., for consignment / picking of goods. The positioning table is placed at three partly overlapping positions (T1, T2, T3) in three consecutive measurement runs and two readers, each having two antennas (at $\mathbf{p}_1$, $\mathbf{p}_2$ & $\mathbf{p}_3$, $\mathbf{p}_4$), are emulated. All antennas are set up at a constant height of 1.3 m.

C. Pre-Processing

The measurement setup in the two described scenarios includes a data processing pipeline comprising the following steps: First, the cross-talk and system-response are removed for calibration of the downlink and the uplink channel measurements. These measurements are subsequently convolved with each other to get the calibrated measurements of the backscatter channel [2]. Next, this backscatter signal is converted to baseband using a center frequency of $f_\mathrm{c} = 900\,\mathrm{MHz}$. Finally, the bandwidth is reduced by convolution with a root-raised-cosine pulse $s(t)$ with a pulse duration of $T_p = 1\,\mathrm{ns}$ and roll-off-factor of 0.6. The result of this pre-processing is called channel response (CR) $\mathbf{g}_{kk'}$ given by

$$\mathbf{g}_{kk'} = \alpha_{kk'}\mathbf{s}_{\tau_{kk'}} + \mathbf{n}_\mathrm{c}. \tag{20}$$

In contrast to the received signal model, the actual signal contains AWGN which is neglected in further considerations due to the high SNR of the employed channel sounder.

Due to the large bandwidth, we can assume that the LOS can be resolved from the multipath components which enables us to estimate $\alpha_{kk'}$ by a projection $\hat{\alpha}_{kk'} = \mathbf{g}_{kk'}^H \mathbf{s}_{\tau_{kk',\mathrm{GM}}} T_s$ of the CR onto the baseband pulse at the true delay given by the geometric model $\tau_{kk',\mathrm{GM}} = (\|\mathbf{p}_{\ell k} - \mathbf{p}\| + \|\mathbf{p} - \mathbf{p}_{\ell' k'}\|)/c$. This estimate is used for the following channel analysis.

V. Channel Analysis

In order to investigate the properties of the backscatter channel with a focus on ranging and positioning, we consider the following three parameters for the analysis:

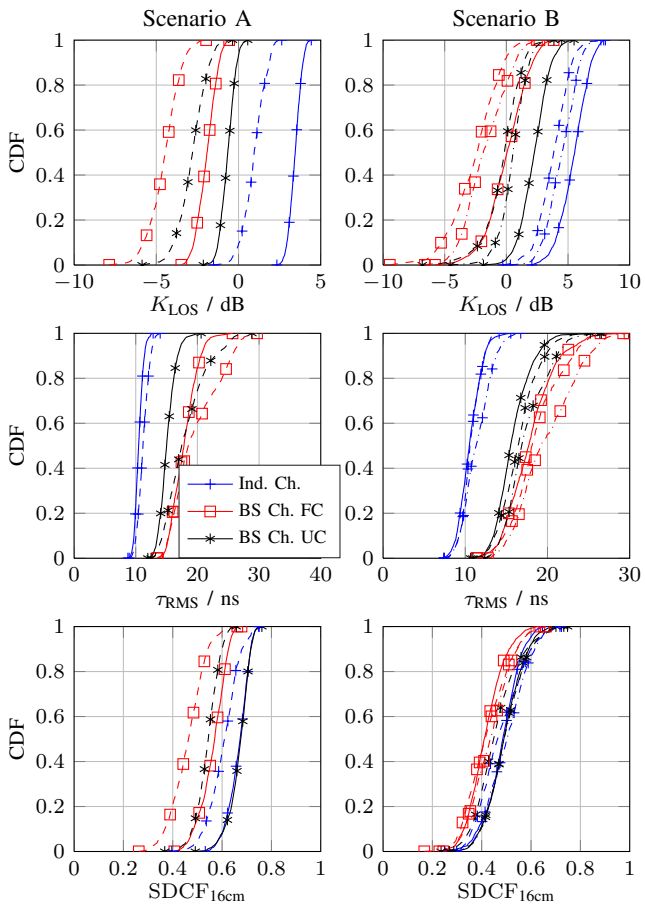

Fig. 3. Cumulative distribution functions (CDF) of the three parameters (1st row K_{LOS}, 2nd row τ_{RMS}, 3rd row SDCF$_{16\mathrm{cm}}$) for both individual (Ind.) and backscatter (BS) channels for Scenario A (left column) and Scenario B (right column). The different line types distinguish the table positions (solid lines: T1, dashed lines: T2, dash-dotted lines: T3). Additionally the BS channels are separated into fully correlated (FC) and uncorrelated channels (UC).

Rician K-factor of the LOS component: The ranging performance is highly influenced by the power ratio between the LOS component and all NLOS components [24]. This power ratio is comparable to the Rician K-factor in narrowband systems and is termed Rician K-factor of the LOS component K_{LOS}. Instantaneous K_{LOS} values are computed from individual CRs by $\hat{K}_{\mathrm{LOS},kk'} = \frac{\|\hat{\alpha}_{kk'}\mathbf{s}_{\tau_{kk',\mathrm{GM}}}\|^2}{\|\mathbf{g}_{kk'}-\hat{\alpha}_{kk'}\mathbf{s}_{\tau_{kk',\mathrm{GM}}}\|^2}$.

Root-mean-square delay spread τ_{RMS}: The rms delay spread quantifies the variance of the arrival times of MPCs with significant energy and is estimated from the second centralized moment of instantaneous normalized PDPs including the LOS component, i.e., $|\mathbf{g}_{kk'}|^2$.

Spaced-distance-correlation-function: For methods that exploit spatial diversity (e.g., beamforming, combining of measurements from closely-spaced antennas), uncorrelated measurements are usually preferred to get additional information [8]. We analyze the spaced-distance-correlation-function (SDCF) of the DM which expresses the percentage of correlation at a certain distance. To compute the SDCF for a specific backscatter channel and a specific grid point $\mathbf{p}_{\mathrm{c}}$, we find all points around $\mathbf{p}_{\mathrm{c}}$ on the grid with a certain distance (e.g. $16 \pm 2\,\mathrm{cm}$), $\mathcal{P}_c = \{\mathbf{p}_i : \|\mathbf{p}_i - \mathbf{p}_c\| = 16 \pm 2\,\mathrm{cm}\}$, shift the CRs along time domain such that the LOS delay coincides with the LOS of the center point $\mathbf{p}_c$, estimate the mean of the complex channel coefficients for the LOS component, subsequently subtract the LOS component, compute the correlation coefficients between the channel transfer functions of the DM at $\mathbf{p}_{\mathrm{c}}$ with all $\mathbf{p}_i$, and average over all points in $\mathcal{P}_c$. In Section III-B the overall covariance matrix is approximated with a diagonal block matrix. This means, that correlations between the individual antenna elements are neglected. The lower the SDCF for the DM is, the better this approximation holds.

We evaluate the described parameters for all individual channels and all backscatter channels, and discuss the results and their implications for the ranging problem (for the two scenarios described in Section IV). The channel-analysis results are shown in Fig. 3 as cumulative distribution functions (CDF). The left column shows the results for Scenario A and the right for Scenario B.

A. Analysis for Scenario A

Solid and dashed lines are table positions T1 and T2 respectively. The backscatter channel results, which are separated in fully correlated (FC - red and squares) channels (downlink =uplink / $\ell = \ell'$ and $k = k'$) and (partly) uncorrelated (UC - black and asterisks) channels ($\ell \neq \ell'$ or $k \neq k'$), and the individual (Ind. - blue and crosses) channel (downlinks/uplinks) results are depicted.

The K_{LOS} factor (in dB) for the individual channels is always positive for T1 (median of $4.2\,\mathrm{dB}$), while for T2 it is positive for $80\,\%$ of the measurements (median of $0.9\,\mathrm{dB}$). This reduction is explained by the larger distance to T2 since the power in the LOS component decreases faster than the power in the NLOS components. According to theory [2] the Rician K-factor for the LOS component of a backscatter channel is

$$K_{\mathrm{LOS},kk'} = \left(1 - \frac{\kappa}{2}\right) \frac{K_{\mathrm{LOS},k} K_{\mathrm{LOS},k'}}{1 + K_{\mathrm{LOS},k} + K_{\mathrm{LOS},k'}}, \qquad (21)$$

with κ as correlation coefficient ranging from 0 to 1 for uncorrelated and fully correlated channels respectively, and $K_{\mathrm{LOS},k}$ and $K_{\mathrm{LOS},k'}$ as the Rician K-factor for the individual constituent channels. Equ. (21) shows that the backscatter K_{LOS} factor is dominated by the smaller of the two individual factors and that for fully correlated individual channels, a $3\,\mathrm{dB}$ loss is expected compared to uncorrelated channels. In Fig. 3, this loss is only $2\,\mathrm{dB}$ because the assumption of fully uncorrelated channels does not hold true within this set-up.

The RMS delay spread for the individual channels is slightly larger for T2 explained by the same reasoning as above, that the LOS component attenuates faster with increasing distance than the NLOS components. The RMS delay spread is larger for the backscatter channels since the delays are extended by the convolution of the channels. The FC data have a larger RMS delay spread than the UC data because the power in the NLOS component is increased up to a factor of two.

The median of the SDCF evaluated at a spacing of $16\,\mathrm{cm}$ is 0.7 for both individual and the uncorrelated backscatter channels, and below 0.4 to 0.5 for the fully correlated

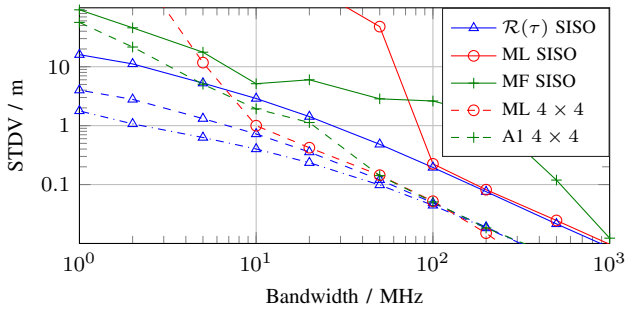

(a)

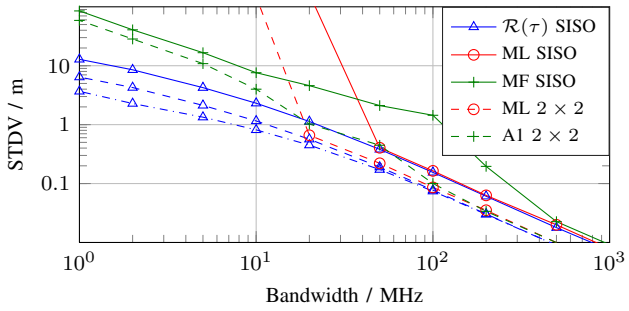

(b)

Fig. 4. REB (blue, triangles) for SISO (solid), MIMO (dashed) according to (17) and MIMO including the effect of the PDP (dash dotted) according to (16), and range estimation standard deviations of the developed algorithms for simulated data (solid lines: SISO, dashed lines: MIMO). The PDP of the downlink and uplink have been modeled with a double exp. PDP [4] leading to the following channel parameters:
(a) Scenario A: $K_{\mathrm{LOS}} = -3\,\mathrm{dB}$, $\tau_{\mathrm{RMS}} = 18.6\,\mathrm{ns}$.
(b) Scenario B: $K_{\mathrm{LOS}} = 0.2\,\mathrm{dB}$, $\tau_{\mathrm{RMS}} = 18.4\,\mathrm{ns}$.

backscatter channels. With increasing distance (cmp. T1 and T2) the correlation of the DM is slightly reduced for both the individual and the backscatter channels by a value of approximately 0.1.

B. Analysis for Scenario B

Solid, dashed, and dash-dotted lines are table positions T1, T2, and T3 respectively. The results compare well to the data gathered in the laboratory. The K_{LOS} factor for individual channels again exceeds $0\,\mathrm{dB}$ (median of $5\,\mathrm{dB}$) and the results for the backscatter channel are slightly above the K_{LOS} factor obtained in the laboratory due to the shorter distances. The median of the RMS delay spread is $17\,\mathrm{ns}$ for the backscatter and $11\,\mathrm{ns}$ for the individual channels. The median of the SDCF evaluated at $16\,\mathrm{cm}$ is 0.4 for the FC backscatter and 0.5 for the individual and UC backscatter channels. The results for the different table positions are in general more homogeneous than for the laboratory scenario, since the table positions are partly overlapping.

VI. Validation of the Algorithms

We finally validate the algorithms presented in Sec. III with simulated and measured data over a wide range of bandwidths.

A. Simulated Data

The algorithms are validated using simulated data, generated according to the estimated channel parameters (K_{LOS} and τ_{RMS}) from Section V. Fig. 4 shows the REBs for the SISO (blue, solid line) and MIMO model (blue, dashed line) according to (17), as well as the REB for the MIMO model including the effect of the PDP (blue, dash-dotted line) according to (16). For Scenario A and Scenario B a 4×4 and 2×2 MIMO setup is used respectively. The effect of including the PDP dependent part in the REB is only relevant at lower bandwidths (BWs). Furthermore, the standard deviations for different estimators are depicted in Fig. 4:

- ML SISO (red solid, 'o'): The SISO ML estimator (5) is able to follow the REB to BWs in the range of $50-100\,\mathrm{MHz}$. At smaller BW the risk of large outliers is high, as the SINR, which determines the detectability of the LOS after whitening, is small.[14]
- MF SISO (green solid, '+'): The SISO MF estimator (7) does not consider the DM and deviates from the bound already at large BW. At small BW the MF estimator gets more robust than the ML, as the complete power of the PDP overlaps with the arrival of the LOS, and the estimator can *make use* of this power. However, the ranging precision is only in the range of the distance between the transmitting reader, the tag and the receiving reader (or higher).
- ML MIMO (red dashed, 'o'): In Section III-C it was argued that (18) is the REB for a MIMO setup with knowledge of the PDP and the AoD and AoA. To show that with this knowledge, the actual REB can be achieved, we use the following technique: We compute the log-likelihoods according to (4) (needing to know the DM) align them in time-domain with respect to the array positions (needing to know the AoD and AoA for the delay-sum beamformer) and take the sum over all array positions. In Fig. 4 two gains are seen for the ML MIMO estimator, (i) a precision gain at constant bandwidth, and (ii) a detection gain, as the estimator is able to follow the bound to smaller BWs compared to the ML SISO estimator.
- A1 MIMO (green dashed, '+'): The MIMO estimator applying Algorithm 1 is able to achieve the MIMO REB at large BWs. It deviates from the bound at larger BWs than the ML MIMO estimator, since the estimation of the parameters of the DM, the AoD and the AoA reduces the EFI. Interestingly, the estimator does not show the high level of outliers as the ML estimators. This can be argued in the following way: During the initialization of the algorithm, a grid search is performed which is closely related to an MF estimator. As the MF estimator does not take the DM process into account, some power of the DM process is included in the initial LOS estimate. The subsequent DM estimation procedure underestimates the power included in the DM. At small BWs (below $10\,\mathrm{MHz}$) most of the DM interferes with the LOS component and thus most of the DM power is included in the LOS initialization. Thus, Algorithm 1 converges towards a matched filter implementation at small BW.

B. Measured Data

To be able to compute the REB, the associated parameters, and the ML estimators, the covariance matrix of the DM

[14] see dashed lines in Fig. 5 and explanation below.

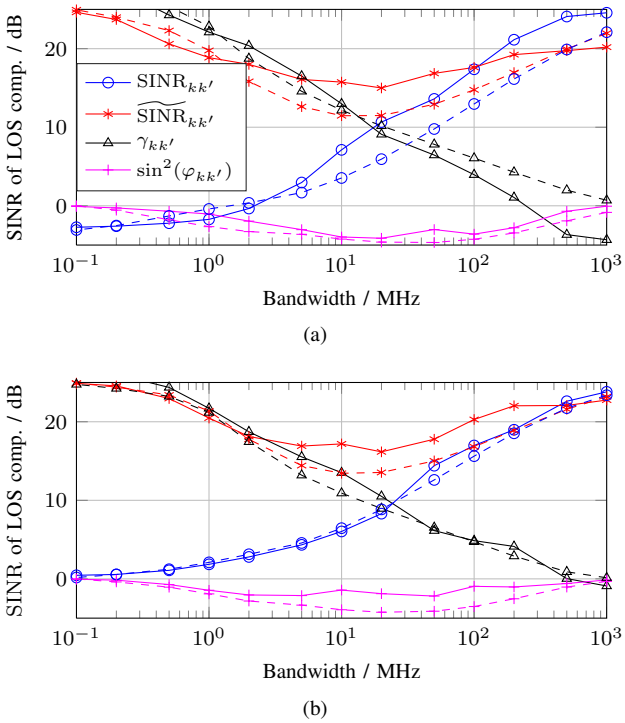

Fig. 5. $\mathrm{SINR}_{kk'}$, $\widetilde{\mathrm{SINR}}_{kk'}$, whitening gain $\gamma_{kk'}$, and information loss $\sin^2(\varphi_{kk'})$ for measured (solid lines) and simulated data (dashed lines).
(a) Scenario A: measured data (solid lines / TX antenna at $\mathbf{p}_1$, table position T2, RX antenna at $\mathbf{p}_2$ / $K_{\mathrm{LOS}} = -3\,\mathrm{dB}$, $\tau_{\mathrm{RMS}} = 18.3\,\mathrm{ns}$) and simulated data (dashed lines / channel parameters see Fig. 4a).
(b) Scenario B: measured data (solid lines / TX antenna at $\mathbf{p}_2$, table position T3, RX antenna at $\mathbf{p}_4$ / $K_{\mathrm{LOS}} = 0.22\,\mathrm{dB}$, $\tau_{\mathrm{RMS}} = 18.2\,\mathrm{ns}$) and simulated data (dashed lines / channel parameters see Fig. 4b).

process needs to be estimated from the measured data.

1) Covariance Estimation: The covariance matrix is determined as follows.[15] At each table position, the overall 18×17 grid is reduced to smaller subgrids (5×5), leading to $N_{\mathrm{sg}} = 9$ non-overlapping subgrids. This reduction of the grid is necessary since the covariance matrix of DM is position dependent. The following processing steps are conducted:

- Extract channel responses $\mathbf{g}_{kk',1\,\mathrm{GHz}}$ at the largest possible bandwidth (1 GHz) on a subgrid.
- Align the channel responses such that the LOS components arrive at the same time $\tau_{kk'}$.
- Estimate the complex channel coefficients $\hat{\alpha}_{kk'}$ with the projection of the CR onto the baseband pulse $\mathbf{s}_{\tau_{kk'}}$.
- Compute the mean value of the estimated complex channel coefficients $\bar{\hat{\alpha}}_{kk'}$.
- At the target bandwidth, extract channel responses $\mathbf{g}_{kk'}$, align the signals such that the LOS components arrive at the same time, subtract the LOS signal $\bar{\hat{\alpha}}_{kk'}\mathbf{s}_{\tau_{kk'}}$ and compute the covariance matrix of the resulting signals.
- To arrive at the covariance matrix for DM plus AWGN we need to add the noise variance N_0/T_{s} to the main diagonal. We define N_0 via the energy of the LOS component $E_{\mathrm{LOS}} = |\bar{\hat{\alpha}}_{kk'}|^2 \|\mathbf{s}_{\tau_{kk'}}\|^2 T_{\mathrm{s}}$. The SNR for the LOS component is set to $E_{\mathrm{LOS}}/N_0 = 25\,\mathrm{dB}$ for the following validation.

[15]The estimation of the covariance matrix as described here is for the validation of the REB only. It is not a practical algorithm to be used in actual ranging / positioning applications due to its requirement of the LOS amplitudes.

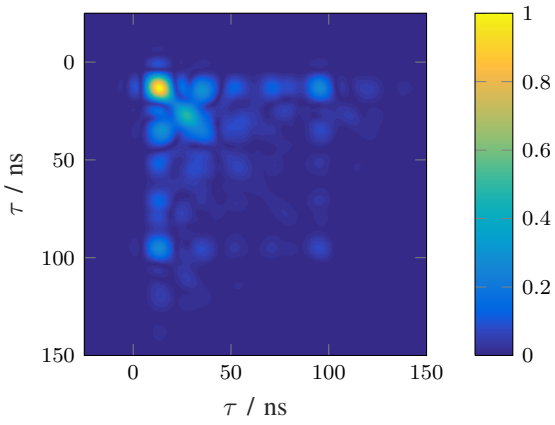

Fig. 6. Estimated covariance matrix of DM at $B = 100\,\mathrm{MHz}$ for the backscatter channel from antenna 1 via tag 1 to antenna 1 measured in the laboratory scenario. For improved illustration, the absolute values scaled to the range 0 -1 are shown.

The resulting covariance matrix estimate is shown in Fig. 6 for a BW of 100 MHz. For the plot, the signals are shifted such that the LOS components arrive at 0 ns. The resulting estimate shows that the US assumption does not hold for the considered scenario. The off-diagonal terms stem from deterministic reflections at flat surfaces which are correlated via the room geometry.

2) Evaluation and Comparison to Simulated Data: To be able to apply the developed estimators to the acquired measurement data, we use the pre-processing steps laid out in Sec. IV-C to derive the CRs at the target bandwidth, and add AWGN (generated with the previously defined N_0) to obtain the received signal described in (3).

In Fig. 5, the $\mathrm{SINR}_{kk'}$, effective SINR $\widetilde{\mathrm{SINR}}_{kk'}$, whitening gain $\gamma_{kk'}$ and information loss $\sin^2(\varphi_{kk'})$ are shown for different bandwidths for both scenarios (solid lines). The SINR tends towards the SNR and towards the K_{LOS} factor for large and small bandwidth respectively. In comparison, the effective SINR is achieving the SNR also at small bandwidth. The $\mathrm{SINR}_{kk'}$ and $\widetilde{\mathrm{SINR}}_{kk'}$ describe the amplitude fading and the pulse distortion of the LOS component respectively [11]. At very large bandwidth neither pulse distortion nor amplitude fading occur as the DM is resolved from the LOS component. At small bandwidth only "flat" amplitude fading occurs as the complete DM overlaps with the LOS component. In-between these two extreme cases, both effects occur and deteriorate the ranging precision which is described by $\widetilde{\mathrm{SINR}}_{kk'}$. The two factors linking the $\mathrm{SINR}_{kk'}$ and $\widetilde{\mathrm{SINR}}_{kk'}$ are the whitening gain $\gamma_{kk'}$ and the information loss $\sin^2(\varphi_{kk'})$. In both scenarios, the comparison to simulated data (dashed lines) shows an excellent match over the entire considered bandwidth range. The main difference is the negative whitening gain at large bandwidths in Fig. 5a which is explained by a frequency dependent behavior of the antenna pattern. The useful bandwidth in this case is actually smaller than 1 GHz explaining the negative whitening gain. As the bandwidth gets smaller, the frequency

Table I: Summary of the achievable REB and standard deviations of the MF and A1 estimators for three different operating scenarios (SISO, 2x2 MIMO & 4x4 MIMO) at three different bandwidths (regulations of the ETSI (EU), FCC (US) and for operation in the 2.4 GHz ISM band) in m. The REB has been simulated with the parameters given in Fig. 5b for the SISO and 2×2 MIMO case and the parameters given in Fig. 5a for the 4×4 MIMO case.

	ETSI 3 MHz	FCC 26 MHz	ISM 83.5 MHz
REB SISO	3.68	0.70	0.19
MF SISO	3.47	0.86	0.35
REB MIMO 2x2	1.84	0.35	0.09
A1 MIMO 2x2	1.85	0.32	0.11
REB MIMO 4x4	0.86	0.19	0.06
A1 MIMO 4x4	2.08	0.52	0.18

dependent behavior vanishes and the simulated data fits the actual measurements. In Scenario B, this effect is not visible due to the different geometric setup.

In Fig. 7, the REB and the standard deviations of the introduced estimators are shown for a SISO and MIMO ranging scenario. The REB including the effect of the PDP cannot be computed, as the US assumption (off-diagonal terms in the covariance matrix, cf. Fig. 6) is violated. The same four estimators as in Fig. 4 are analyzed:

- ML SISO (red solid, 'o'): The SISO ML estimator is able to follow the REB to BWs in the region of 50 MHz again and shows the high risk of outliers below this BW.
- MF SISO (green solid, '+'): The SISO MF estimator deviates from the REB at high BWs, and gets more robust than the ML at lower BWs, just as in the simulations. At BWs below 10 MHz, in Scenario B, it outperforms the REB which can be explained since the REB does not consider the second term in (16), leading in turn to a too high REB (cf. Fig. 4).
- ML MIMO (red dashed, 'o'): The MIMO ML estimator shows a similar behavior as in the simulations. In Fig. 7a, it starts to deviate from the bound at 50 MHz but does not show the high risk of outliers down to a BW of 10 MHz. This can be attributed to the off-diagonal terms in the covariance matrix (violation of US assumption).
- A1 MIMO (green dashed, '+'): The developed algorithm for the MIMO setup does not achieve the bound at very high BWs because the LOS-plus-DM channel model is not correct at these BWs. Here, a channel model consisting of more than one distinct specular component plus DM (a so-called geometry-based stochastic channel model [25]) should be employed. At a bandwidth below 100 MHz the algorithm starts to achieve the bound since the LOS plus DM model starts to fit the measured data better. At even lower BWs, the algorithm starts to outperform not only the MIMO ML estimator but also the REB for the MIMO case (in Scenario B). As Algorithm 1 tends towards an MF algorithm at small BWs it makes use of the DM process, hence it outperforms the MIMO ML estimator. The REB in Fig. 7 does not take the delay information of the DM process into account, which is the reason that the algorithm can outperform the REB.

In Table I an overview of the achievable ranging precision is listed for three different operating scenarios (Scenario B; SISO, 2x2 MIMO & Scenario A; 4x4 MIMO) at three different BW. The BW are chosen to fit into the ETSI and FCC regulations for UHF RFID systems and the 2.4 GHz ISM band.

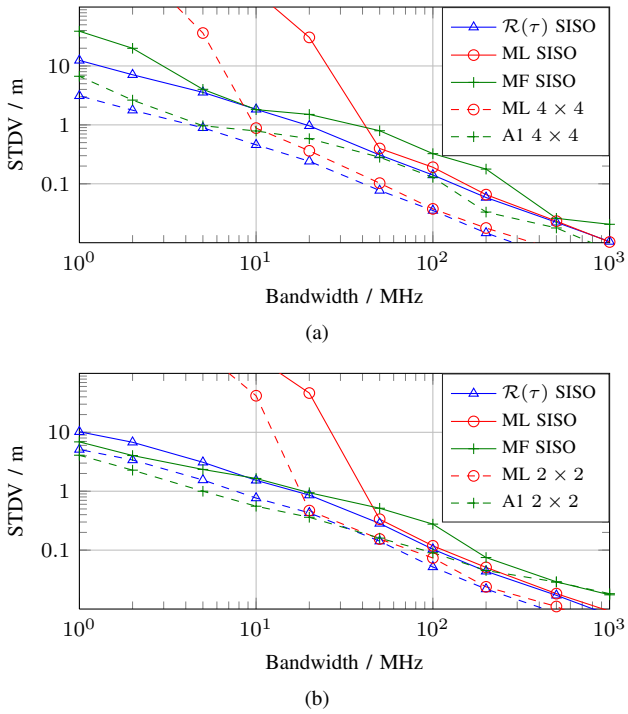

Fig. 7. REB and range estimation standard deviations for measured data (solid lines: SISO, dashed lines: MIMO). The REB (blue, triangles) is depicted for the SISO and MIMO setup according to (17). Non-practical algorithms (need to know the PDP of the DM) are shown with 'o'. Practical algorithms are shown with '+'. (a) Scenario A, (b) Scenario B.

At each BW the estimators, MF for the SISO case and A1 for the MIMO case, are compared to the REB. Interestingly, the estimator performs better for the 2×2 than the 4×4 MIMO setup. This can be explained by (i) the "better" channel parameters with respect to ranging of Scenario B [24] and (ii) the shortcomings of the algorithm: it does not take the correlations of the DM into account and assumes that the complex amplitudes as well as the DM are the same for all backscatter channels.[16] For a 2×2 setup, the ranging precision is 1.85, 0.35 and 0.11 m in the ETSI, the FCC and the ISM band respectively.

VII. Conclusions

We analyzed channel measurements in the UHF-RFID frequency band, obtained in two different environments, a laboratory and an industrial hall. Wideband channel parameters have been analyzed, the Rician K-factor for the LOS component, the RMS delay spread, and the spaced distance correlation function. These parameters influence the achievable ranging performance which can be quantified with a Cramér Rao lower bound. This bound on the ranging error standard deviation has been validated with two algorithms which need to know the statistics of the DM with simulated data and measured data. Furthermore, two practical algorithms have been developed, (i) a naïve matched filter estimator for the SISO setup and (ii) an iterative algorithm for the MIMO setup capable of estimating the parameters of the LOS and the parameters of the

[16] As the antennas emulating an RFID reader are spaced by 20 cm these assumptions start to be violated.

DM. For a MIMO system the precision is below 20 cm at a bandwidth of 83.5 MHz which fits in the ISM band. Future research will focus on validating the developed algorithms with measurements including a real UHF-RFID tag.

APPENDIX

This appendix derives the update equations for the MIMO algorithm presented in Section III-B. Inserting the structured mean field approximation (10) into the variational lower bound given in (11) one can show that [21]

$$\mathcal{L}(q) = -\mathrm{KL}(q(\boldsymbol{\psi})||\tilde{f}(\boldsymbol{\psi})) + \text{const.} \tag{22}$$

with KL as Kullback-Leibler divergence and

$$\tilde{f}(\boldsymbol{\psi}) = \frac{\exp(\mathbb{E}_{q(\boldsymbol{\eta})q(\alpha)}\{\log f(\boldsymbol{\theta}_{\mathrm{MIMO}}, \mathbf{r})\})}{\int \exp(\mathbb{E}_{q(\boldsymbol{\eta})q(\alpha)}\{\log f(\boldsymbol{\theta}_{\mathrm{MIMO}}, \mathbf{r})\}) d\boldsymbol{\psi}}. \tag{23}$$

By choosing a point estimate for the parameters $q(\boldsymbol{\psi}) = \delta(\boldsymbol{\psi} - \hat{\boldsymbol{\psi}})$ we find from (22)

$$\begin{aligned}
\hat{\boldsymbol{\psi}}^{\text{new}} &= \underset{\hat{\boldsymbol{\psi}}}{\operatorname{argmin}} \left\{ \mathrm{KL}(\delta(\boldsymbol{\psi} - \hat{\boldsymbol{\psi}})||\tilde{f}(\boldsymbol{\psi})) \right\} = \underset{\hat{\boldsymbol{\psi}}}{\operatorname{argmax}} \left\{ \log \tilde{f}(\hat{\boldsymbol{\psi}}) \right\} \\
&= \underset{\hat{\boldsymbol{\psi}}}{\operatorname{argmax}} \left\{ \mathbb{E}_{q(\boldsymbol{\eta})q(\alpha)} \left\{ \log f(\hat{\boldsymbol{\psi}}, \boldsymbol{\eta}, \alpha, \mathbf{r}) \right\} \right\} \qquad (24) \\
&= \underset{\hat{\boldsymbol{\psi}}}{\operatorname{argmax}} \left\{ \mathbb{E}_{q(\boldsymbol{\eta})q(\alpha)} \left\{ \log \left(f(\mathbf{r}|\hat{\boldsymbol{\psi}}, \boldsymbol{\eta}, \alpha) f(\hat{\boldsymbol{\psi}}) \right) \right\} \right\} + \text{const.}
\end{aligned}$$

We thus have to solve for the expectation operator in (24). This is done by choosing point estimates for the AWGN, the DM parameters $q(\boldsymbol{\eta}) = \delta(\boldsymbol{\eta} - \hat{\boldsymbol{\eta}})$, and the complex amplitudes $q(\alpha) = \delta(\alpha - \hat{\alpha})$. Since we have no prior information regarding the parameters, a uniform prior is chosen, leading to the update equation for the LOS parameters

$$\hat{\boldsymbol{\psi}}^{\text{new}} = \underset{\hat{\boldsymbol{\psi}}}{\operatorname{argmax}} \left\{ - \left(\mathbf{r} - \hat{\alpha}\mathbf{s}(\hat{\boldsymbol{\psi}}) \right)^H \mathbf{C}(\hat{\boldsymbol{\eta}})^{-1} \left(\mathbf{r} - \hat{\alpha}\mathbf{s}(\hat{\boldsymbol{\psi}}) \right) \right\}.$$

By performing the same steps for the complex amplitude, (24) reads

$$\begin{aligned}
\hat{\alpha}^{\text{new}} &= \underset{\hat{\alpha}}{\operatorname{argmax}} \left\{ \mathbb{E}_{q(\boldsymbol{\eta})q(\boldsymbol{\theta})} \{ \log \left(f(\mathbf{r}|\boldsymbol{\psi}, \boldsymbol{\eta}, \hat{\alpha}) f(\hat{\alpha}) \right) \} \right\} + \text{const.} \\
&= \underset{\hat{\alpha}}{\operatorname{argmax}} \left\{ - \left(\mathbf{r} - \hat{\alpha}\mathbf{s}(\hat{\boldsymbol{\psi}}) \right)^H \mathbf{C}(\hat{\boldsymbol{\eta}})^{-1} \left(\mathbf{r} - \hat{\alpha}\mathbf{s}(\hat{\boldsymbol{\psi}}) \right) \right\}
\end{aligned} \tag{25}$$

As $\hat{\alpha}$ appears linearly in (25), the maximum can be found analytically as

$$\hat{\alpha}^{\text{new}} = \frac{\mathbf{r}^H \mathbf{C}(\hat{\boldsymbol{\eta}})^{-1} \mathbf{s}(\hat{\boldsymbol{\psi}})}{\mathbf{s}(\hat{\boldsymbol{\psi}})^H \mathbf{C}(\hat{\boldsymbol{\eta}})^{-1} \mathbf{s}(\hat{\boldsymbol{\psi}})}. \tag{26}$$

For the noise parameters, (24) reads

$$\begin{aligned}
\hat{\boldsymbol{\eta}}^{\text{new}} &= \underset{\hat{\boldsymbol{\eta}}}{\operatorname{argmax}} \left\{ \mathbb{E}_{q(\boldsymbol{\psi})q(\alpha)} \{ \log \left(f(\mathbf{r}|\boldsymbol{\psi}, \hat{\boldsymbol{\eta}}, \alpha) f(\hat{\boldsymbol{\eta}}) \right) \} \right\} + \text{const} \\
&= \underset{\hat{\boldsymbol{\eta}}}{\operatorname{argmax}} \left\{ - \log \{ |\mathbf{C}(\hat{\boldsymbol{\eta}})| \} \right. \qquad (27) \\
&\quad \left. - \left(\mathbf{r} - \hat{\alpha}\mathbf{s}(\hat{\boldsymbol{\psi}}) \right)^H \mathbf{C}(\hat{\boldsymbol{\eta}})^{-1} \left(\mathbf{r} - \hat{\alpha}\mathbf{s}(\hat{\boldsymbol{\psi}}) \right) \right\},
\end{aligned}$$

where the last equality is again due to the assumption of a uniform prior for the noise parameters.

Finally, during the initialization of the algorithm it is assumed, that only AWGN is present to initialize the power spectral density N_0 and the power of the DM P_{DM}. By reducing the noise parameter vector to $\boldsymbol{\eta} = N_0$ only, and solving (24) again, an analytical solution can be found as

$$\hat{N}_0 = \frac{T_s \left(\mathbf{r} - \hat{\alpha}\mathbf{s}(\hat{\boldsymbol{\psi}}) \right)^H \left(\mathbf{r} - \hat{\alpha}\mathbf{s}(\hat{\boldsymbol{\psi}}) \right)}{NKK'}. \tag{28}$$

REFERENCES

[1] J. D. Griffin and G. D. Durgin, "Gains for RF tags using multiple antennas," *IEEE Trans. Antennas Propag.*, vol. 56, no. 2, pp. 563–570, Feb. 2008.

[2] D. Arnitz, U. Muehlmann, and K. Witrisal, "Wideband characterization of backscatter channels: Derivations and theoretical background," *IEEE Trans. Antennas Propag.*, vol. 60, no. 1, pp. 257–266, Jan. 2012.

[3] M. S. Varela and M. G. Sanchez, "RMS delay and coherence bandwidth measurements in indoor radio channels in the UHF band," *IEEE Trans. Veh. Technol.*, vol. 50, no. 2, pp. 515–525, Mar. 2001.

[4] J. Karedal, S. Wyne, P. Almers, F. Tufvesson, and A. F. Molisch, "A measurement-based statistical model for industrial ultra-wideband channels," *IEEE Trans. Wireless Commun.*, vol. 6, no. 8, pp. 3028–3037, Aug. 2007.

[5] A. G. Dimitriou, S. Siachalou, A. Bletsas, and J. N. Sahalos, "A site-specific stochastic propagation model for passive UHF RFID," *IEEE Antennas Wireless Propag. Lett.*, vol. 13, pp. 623–626, 2014.

[6] H. Arthaber, T. Faseth, and F. Galler, "Spread-spectrum based ranging of passive UHF EPC RFID tags," *IEEE Commun. Lett.*, vol. 19, no. 10, pp. 1734–1737, Oct. 2015.

[7] D. Dardari, R. D'Errico, C. Roblin, A. Sibille, and M. Z. Win, "Ultra-wide bandwidth RFID: The next generation?" *Proc. IEEE*, vol. 98, no. 9, pp. 1570–1582, Sep. 2010.

[8] S. Hinteregger, E. Leitinger, P. Meissner, and K. Witrisal, "MIMO gain and bandwidth scaling for RFID positioning in dense multipath channels," in *2016 IEEE Int. Conf. RFID*, May 2016, pp. 1–6.

[9] D. Dardari, A. Conti, U. Ferner, A. Giorgetti, and M. Z. Win, "Ranging with ultrawide bandwidth signals in multipath environments," *Proc. IEEE*, vol. 97, no. 2, pp. 404–426, Feb. 2009.

[10] Y. Shen and M. Z. Win, "Fundamental limits of wideband localization-part I: A general framework," *IEEE Trans. Inf. Theory*, vol. 56, no. 10, pp. 4956–4980, Oct. 2010.

[11] K. Witrisal, E. Leitinger, S. Hinteregger, and P. Meissner, "Bandwidth scaling and diversity gain for ranging and positioning in dense multipath channels," *IEEE Wireless Commun. Lett.*, vol. 5, no. 4, pp. 396–399, Aug. 2016.

[12] A. P. Dempster, N. M. Laird, and D. B. Rubin, "Maximum likelihood from incomplete data via the EM algorithm," *J, Roy. Statist., Ser. B*, vol. 39, no. 1, pp. 1–38, 1977.

[13] B. H. Fleury, M. Tschudin, R. Heddergott, D. Dahlhaus, and K. I. Pedersen, "Channel parameter estimation in mobile radio environments using SAGE algorithm," *IEEE J. Sel. Areas Commun.*, vol. 17, no. 3, pp. 434–450, Mar. 1999.

[14] A. Richter, "Estimation of radio channel paramters: Models and algorithms," Ph.D. dissertation, Technische Universitaet Ilmenau, 2005.

[15] D. Arnitz, U. Muehlmann, and K. Witrisal, "Characterization and modeling of UHF RFID channels for ranging and localization," *IEEE Trans. Antennas Propag.*, vol. 60, no. 5, pp. 2491–2501, May 2012.

[16] S. Hinteregger, J. Kulmer, M. Goller, F. Galler, H. Arthaber, and K. Witrisal, "UHF-RFID backscatter channel analysis for accurate wideband ranging," in *2017 IEEE Int. Conf. RFID*, May 2017, pp. 117–123.

[17] A. F. Molisch, "Ultra-wide-band propagation channels," *Proc. IEEE*, vol. 97, no. 2, pp. 353–371, Feb. 2009.

[18] P. V. Nikitin, K. V. S. Rao, and R. D. Martinez, "Differential RCS of RFID tag," *Electron. Lett.*, vol. 43, no. 8, pp. 431–432, 04 2007.

[19] F. Guidi, "Study of ultra wide band modulated backscattering based RFID systems," Ph.D. dissertation, Ecole Polytechnique Paristech, Universita degli studi di Bologna, 2013.

[20] S. Kay, *Fundamentals of Statistical Signal Processing: Estimation Theory*. Prentice Hall Signal Processing Series, 1993.

[21] C. M. Bishop, *Pattern Recognition and Machine Learning (Information Science and Statistics)*. Secaucus, NJ, USA: Springer-Verlag New York, Inc., 2006.
[22] Ilmsens Channel Sounder. [Online]. Available: http://www.ilmsens.com
[23] Mini Circuits, RC-4SPDT-A18 and RC-1SP4T-A18. [Online]. Available: http://www.minicircuits.com
[24] S. Hinteregger, E. Leitinger, P. Meissner, J. Kulmer, and K. Witrisal, "Bandwidth dependence of the ranging error variance in dense multipath," in *2016 24th European Signal Processing Conf. (EUSIPCO)*, Aug. 2016, pp. 733–737.
[25] N. Michelusi, U. Mitra, A. F. Molisch, and M. Zorzi, "UWB sparse/diffuse channels, part I: Channel models and bayesian estimators," *IEEE Trans. Signal Process.*, vol. 60, no. 10, pp. 5307–5319, Oct. 2012.

Stefan Grebien (S'15) received the Dipl.-Ing. degree from the Graz University of Technology, Austria, in 2012.

He joined the Signal Processing and Speech Communication Laboratory, Graz University of Technology in 2015 where he is currently pursuing the Ph.D. degree in electrical engineering. His research interests are estimation theory, Bayesian inference, channel modeling and RFID.

Josef Kulmer (S'15) received the M.Sc. degree in electrical engineering and audio engineering from the University of Music and Performing Arts, Graz, in 2014.

He is currently a Research and Teaching Associate with the Signal Processing and Speech Communication Laboratory, Graz University of Technology, where he is currently pursuing the Ph.D. degree in electrical engineering. His current research interests include linear algebra, exploration of space, and microwaves.

Florian Galler (S'17) received the Dipl.-Ing. degree from TU Wien, Vienna, Austria, in 2014.

He is currently pursuing the Dr.techn. degree with the Microwave Engineering Group at the Institute of Electrodynamics, Microwave, and Circuit Engineering, TU Wien. His current research interests include localization methods for RFID systems and antenna measurements.

Michael Goller received the M.Sc and Ph.D. degrees in Electrical Engineering from the Graz University of Technology, Austria, in 2010 and 2013, respectively.

He has been appointed as the CTO of Detego GmbH (London/Graz, Austria) in 2014, where he is responsible for the development and implementation of the Detego SUITE, a highly scalable software platform for intelligent article management in the fashion retail industry based on the RFID technology. With his strong data and modeling related background, he continuously strives to solve business problems and optimize processes with the help of innovative technology and model driven analysis. His research interests include data driven design and modeling, Bayesian reasoning, and sensor fusion.

Erik Leitinger (S'12–M'16) received the B.Sc., Dipl.-Ing., and Ph.D. (with Highest Hons.) degrees in electrical engineering from the Graz University of Technology, Austria, in 2009, 2012, and 2016, respectively. He currently holds an "Erwin Schrödinger" Post-Doctoral Fellowship with the Department of Electrical and Information Technology, Lund University. His research interests are in ultra-wideband wireless communication, indoor positioning, Bayesian inference, factor graphs, and estimation/detection theory.

He was a recipient of the Outstanding Award of Excellence of the Federal Ministry of Science, Research and Economy for his Ph.D. Thesis and was honored from Graz University of Technology for the patent with the title, *Method, device and system for indoor localization and tracking using ultrawideband radio signals*. He was finalist in the Best Student Paper Competition at IEEE Radar Conference, USA, Cincinnati in 2014.

Holger Arthaber (S'99–M'04) received the Dipl.-Ing. and Dr.techn. degrees from TU Wien, Vienna, Austria, in 2000 and 2004, respectively.

In 2000, he joined the Microwave Engineering Group, Institute of Electrodynamics, Microwave, and Circuit Engineering, TU Wien, where he has been the Head of the Microwave Engineering Group since 2009. He has authored or coauthored more than 85 contributions to international scientific journals and conferences. His current research interests include digitally driven switched-mode power amplifiers, the advancement of active harmonic load-pull systems, polyharmonic distortion modeling, RF material characterization, ranging/localization of UHF RFID tags, digital predistortion, and various aspects of RF system design.

Klaus Witrisal (S'98–M'03) received the Ph.D. degree from the Delft University of Technology, The Netherlands, in 2002 and the Habilitation degree from the Graz University of Technology, Austria, in 2009, where he is currently an Associate Professor. His research interests are in signal processing for wireless communications, propagation channel modeling, and positioning.

He has been an Associate Editor of the IEEE COMMUNICATIONS LETTERS, a Co-Chair of the TWG "Indoor" of the COST Action IC1004 and the EWG "Localisation and Tracking" of the COST Action CA15104, a leading Chair of the IEEE Workshop on Advances in Network Localization and Navigation, and TPC (Co)-Chair of the Workshop on Positioning, Navigation and Communication.